JOURNAL OF MATERIALS SCIENCE 23 (1988) 2370–2378

# Strength of poly(methyl methacrylate) with indentation flaws

J. E. RITTER, M. R. LIN, T. J. LARDNER*
*Mechanical Engineering Department and *Civil Engineering Department, University of Massachusetts, Amherst, Massachusetts 01003, USA*

Controlled flaws were introduced into poly(methyl methacrylate) samples in the presence of liquid acetone using a Vickers indenter over a range of indentation loads from 100 to 1400 N. Due to the large plastic zone underneath the indenter, the radial crack formed by indentation consisted of two halves, known as Palmqvist cracks, instead of a single semicircular crack. The strengths of the samples were measured in air either immediately following indentation or after a stress-relief anneal. The strength of the as-indented samples was about 6% less than that of the annealed samples; however, the dependence of strength on indentation load was similar for both sets of samples. These results were interpreted in terms of an indentation fracture mechanics model. The analysis is consistent with poly(methyl methacrylate) having a rising fracture toughness with increasing crack size.

## 1. Introduction

Valuable insight into the mechanism of failure from surface flaws in inorganic glasses and ceramics has been provided by studies of an idealized model flaw systems produced by a sharp indentation [1–4]. The main advantage of this approach lies in the ability of predetermining the size and location of the strength-controlling flaw so that the subsequent response of this flaw to applied loading and/or environmental influence can be directly observed. Correlations between the fracture characteristics of indentation flaws to fatigue [5, 6], annealing and ageing [7]. machining [8] and particle impact [9] have been used to establish the general applicability of fracture mechanics concepts to the failure of inorganic glasses and ceramics with typical handling and microstructural flaws.

The essential features of the classical deformation-fracture pattern produced by a sharp indenter (Vickers) are shown in Fig. 1. Dimensions $a$ and $r_p$ represent the scale of the hardness impression and plastic zone, respectively, and are used to quantify the extent of the indenter deformation. Two distinctive crack types, radial and lateral, emanate from the deformation zone and are shown in Fig. 1 as RC and LC. The radial cracks lie in a plane containing the load axis and an impression diagonal and control the strength behaviour. The lateral cracks lie on subsurface planes closely parallel to the surface and are responsible for material removal during a sharp-particle impact. Since the final crack dimensions in inorganic glasses and ceramics are achieved as the indenter is removed, it is believed that the driving force for crack formation must be provided by the residual stresses created by the plastic zone [10]. Detailed fracture mechanics analyses for indentation cracking have been developed and verified experimentally by direct observation of flaw response [3, 10].

In contrast to the above, there has been little research on using indentation to study the failure of brittle polymeric materials. Therefore, the objective of this research was to study the applicability of the indentation technique in characterizing the failure behaviour of poly(methyl methacrylate) (PMMA). For this purpose, strength was measured as a function of indentation load and related to the measured radial crack sizes. PMMA was chosen because it is readily available, brittle, and transparent. This latter property allows direct observation of the flaw response to indentation.

## 2. Experimental procedure

PMMA samples were machined from a Plexiglas sheet (Rohm and Haas, Philadelphia) to dimensions of 20.32 cm length, 2.29 cm width, and with a thickness of 0.95 cm. The prepared specimens were then polished by using 600 grade grinding paper to smooth the surfaces. After polishing, the samples were annealed at 85° C for 8 h [11] to remove all the residual stresses associated with machining and/or polishing. An optical interferoscope was used to search for the existence of the stress fringes to ensure that all the residual stresses had been removed.

Controlled surface flaws were introduced by a Vickers diamond pyramid indenter that was attached to an Instron universal testing machine to provide indentation loads ranging from 100 to 1400 N. All indentations were made at room temperature through a drop of acetone placed on the contact surface during the indent period. Acetone was added to provide an aggressive environment which enhanced crack formation. Such cracking did not occur if indentations


0022–2461/88 $03.00 + .12 

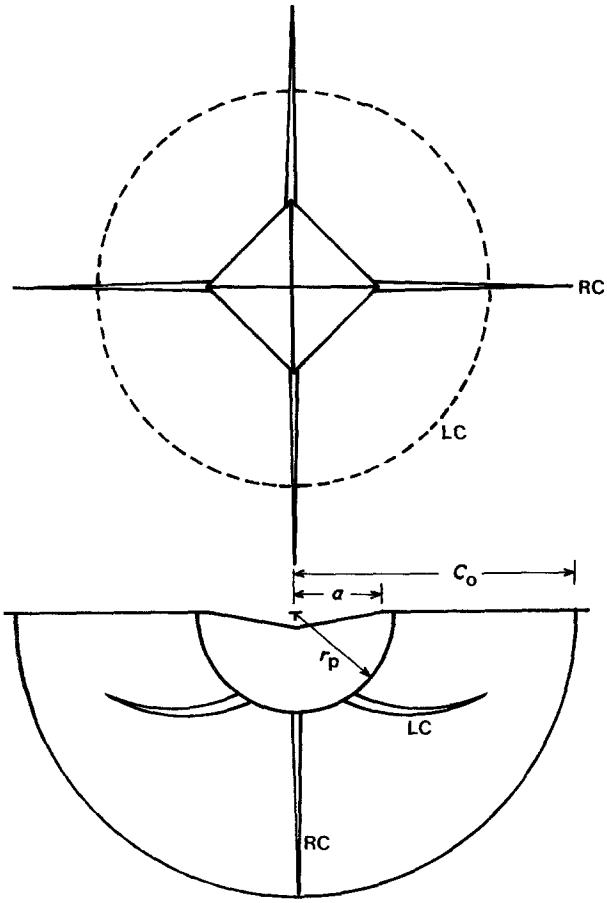


*Figure 1* Top and side views of indentation crack pattern produced by Vickers indenter for general ceramics and inorganic glasses.

were made only in ambient air. The indentation was made with an Instron crosshead speed of 1 mm $min^{-1}$ and a contact time of 12 sec. Care was taken to align radial cracks perpendicular and parallel to the longitudinal axis of the specimen. After indentation the samples were dried and an optical microscope was used to ensure the alignment of the radial cracks and to measure the crack sizes.

Following the measurement of the surface trace of the radial crack, the samples were strength tested either as-indented or annealed. The as-indented tests were conducted immediately after the crack size measurement. Annealing was carried out at 85° C for 8 h following indentation to remove the residual stresses caused by indentation. After annealing, these specimens were rechecked using the optical interferoscope to ensure that they were free of residual stresses. The crack sizes of the annealed specimens were remeasured before strength measurement to make sure no healing or growth occurred during the annealing process.

All strength measurements were performed using a four-point bending fixture with an outer span of 12.7 cm and an inner span of 2.54 cm with the surface containing the indentation flaw on the tension side. The bend test apparatus was designed with several degrees of freedom to minimize any spurious stresses caused by non-uniform specimen dimension and/or beam twisting and was attached to the Instron universal testing machine. All bend tests were conducted in air with a crosshead speed of 1 cm $min^{-1}$. After fracture, the geometrical features of the strength-controlling radial flaw were optically examined to confirm the sites of failure. As expected, all specimens broke from the indentation site and the load–deflection curve from the test was linear until failure. Five specimens were tested for each strength evaluation, from which mean values and standard deviations were computed.

To obtain a measure of the crack growth prior to rupture, an as-indented and an annealed sample were prepared with three indentations (indentation load of 200 N) on their surfaces, spaced about 1 mm apart to avoid influence from each other during testing. The radial cracks, perpendicular to the applied tensile stress, that were on the two indents that did not fail were then assumed to be close to the instability dimension.

Standard single-edged notched three-point bend tests (0.95 cm × 2.29 cm × 10.16 cm) were also performed to obtain a conventional fracture toughness [12] measurement. An initial notch was introduced by using a diamond saw at the centre of one edge. The crack was then sharpened by pushing a razor blade slowly into the saw-cut notch. The samples were checked to ensure that no residual stresses were introduced around the crack tips. The prepared specimens were then tested in three-point bending in air at a crosshead speed of 1 cm $min^{-1}$. Samples were also tested with acetone added and dried in the notch prior to the fracture test to see if acetone could alter the crack tip structure, and hence the subsequent fracture toughness. The three-point bending apparatus had a span of 8.57 cm.

## 3. Results and discussion

### 3.1. Indentation crack morphology

Figs 2a and b show the indentation crack system associated with Vickers indentation of PMMA/acetone at indentation loads of 50 and 200 N, respectively. The surface trace of the radial cracks, RC, emanated from the impression corners and were generated over the entire load range; the secondary cracks, SC, initiated from the impression edges and only formed at loads higher than 100 N. Unlike inorganic glasses and ceramics, lateral cracks were not observed in PMMA over the entire testing range. Close observation revealed that the radial cracks initiated from the intersection points of flow lines within the deformation zone. These flow lines (FL in Fig. 2) are shear bands produced by plastic deformation under the indentor. The shear bands have been observed to be the source of crack initiation in inorganic glasses [13, 14] and in single crystals [15, 16]. Dabbs *et al.* [14] suggested that shear bands generated in different quadrants of the impression can intersect to produce high stress intensification and, thereby, provide favourable sites for radial crack nucleation and growth. This agrees well with the observed PMMA results where radial cracks initiate first from the impression corners. Without the strong shear interaction from different quadrants, secondary cracks are only initiated above a critical load (approximately 100 N in this study) where the inhomogeneous shear stresses produced from the same quadrant can overcome the surface

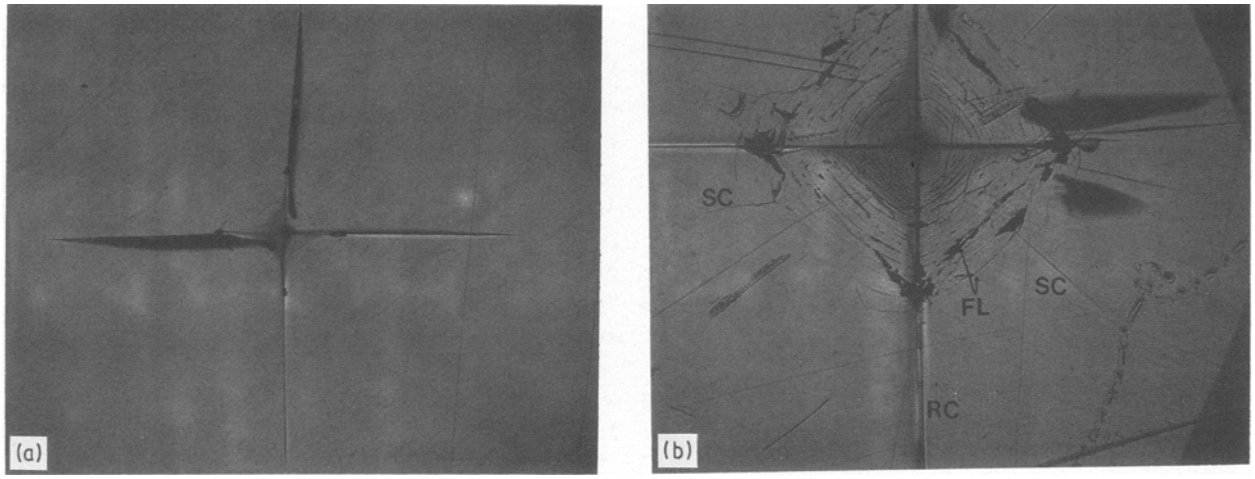


*Figure 2* Indentation cracks for PMMA/acetone at different loads: (a) 50 N (26 ×), (b) 200 N (52 ×).

energy to form cracks. Although this shear-fault mechanism can well describe the crack formation phenomena observed in PMMA/acetone, the associated fracture mechanics model for crack initiation has not been well developed and further research is required to develop a quantitative model.

A schematic cross-sectional view of the radial crack is shown in Fig. 3. It can be seen that the radial crack consists of two "wings" that are separated by a large plastic zone beneath the indentation impression. Such a radial crack pattern is known as Palmqvist crack [17–19] and has been observed to form with Vickers indentations in cemented carbides. Compared to crack patterns generated in inorganic glasses or ceramic materials (Fig. 1), the main difference is the absence of a connection of the radial cracks beneath the impression site. Obviously, in the Palmqvist crack pattern the large plastic zone blocks the coalescence of the two wings of the radial cracks on the median plane in forming a semicircular crack. In view of this observation, the ratio $C_0/r_p$ (Fig. 1) was calculated from the data in the literature for a wide range of brittle materials and correlated with the nature of the radial crack pattern.

The solution for an internally pressurized cavity in an elastic–plastic material gives for the plastic zone size, $r_p$ [20]

$$r_p = a\left(\frac{E}{3Y(1-\nu)}\right)^{1/3} \quad (1)$$

where $E$ is elastic modulus, $Y$ is yield strength, $\nu$ is Poisson's ratio, and $a$ is one-half the indent diagonal. For a Vickers indentor

$$a = (P/2H)^{1/2} \quad (2)$$

where $P$ is the indentation load and $H$ is hardness. The expression for $r_p$ for ceramics and inorganic glasses becomes, upon taking hardness to be $2.5Y$ [14, 22] and $\nu$ to be 0.25 [21, 22],

$$r_p = 0.732E^{1/3}H^{-5/6}P^{1/2} \quad (3)$$

For PMMA hardness is $1.5Y$ [21, 22] and $\nu$ is 0.33 so that $r_p$ is given by

$$r_p = 0.642\,E^{1/3}H^{-5/6}P^{1/2} \quad (4)$$

The hardness of PMMA, as measured from the Vickers microindentation, was 0.21 GPa and was found to be independent of indentation load (100 to 1400 N). The elastic modulus of PMMA was taken to be 3.1 GPa [23].

The equilibrium radial crack size after indentation, $C_0$, as measured by the surface trace of the radial

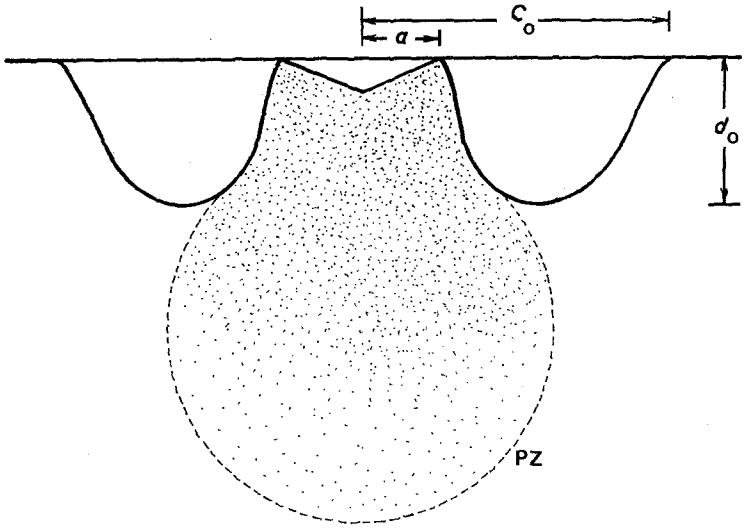


*Figure 3* Schematic cross-section of radial cracks for PMMA.

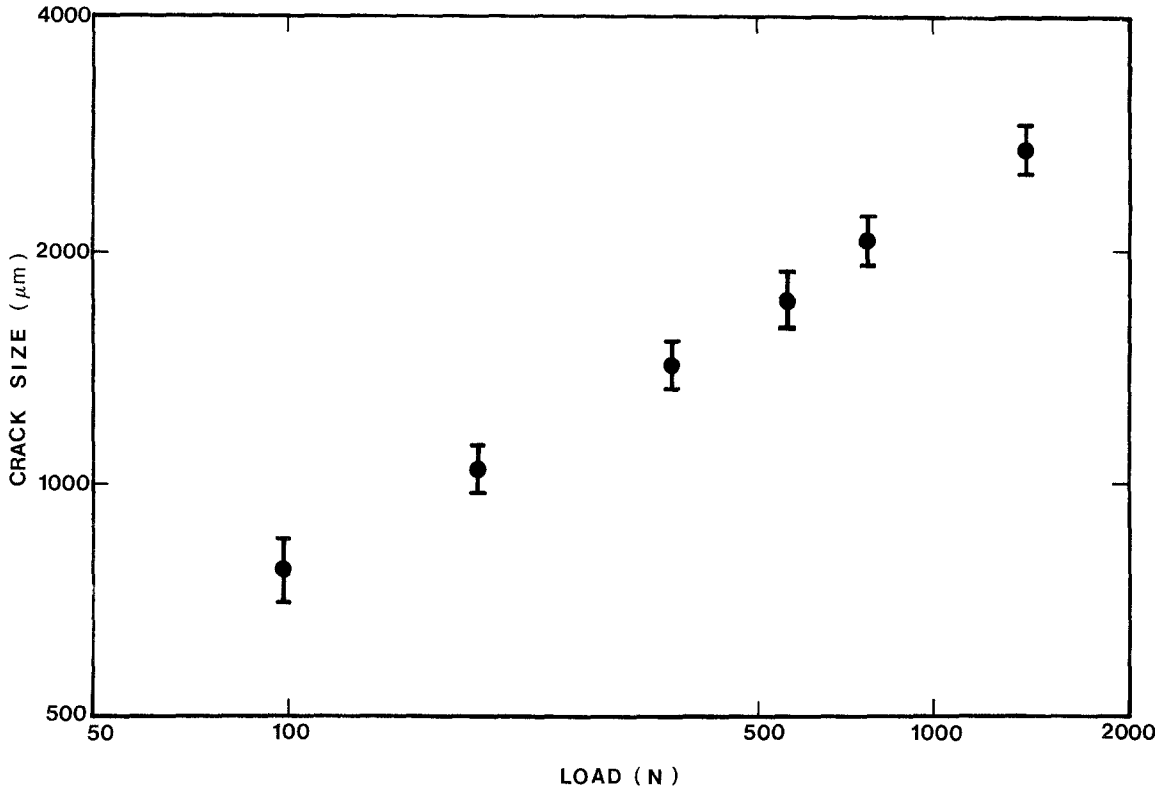


*Figure 4* Surface radial trace against indentation load.

crack, was determined directly from the published values at $P = 100\,N$ for the different materials. In cases where data are not available at $P = 100\,N$, the data were extrapolated. The $C_0/r_p$ ratios are summarized in Table I. It can be clearly seen from these data that when the $C_0/r_p$ ratio becomes greater than 1.0, the radial cracks can connect beneath the plastic zone on the median plane to form a semi-circular flaw. On the other hand, when the $C_0/r_p$ ratios are low (about 0.7 or less) the radial cracks are prevented from joining by the plastic zone.

## 3.2. Crack size–indentation load

The radial crack size, $C_0$, after indentation for PMMA/acetone is plotted on logarithmic axes as a function of the indentation loads in Fig. 4. The best-fit slope of these data is found to be 0.50 ($\pm$0.06). This clearly does not agree with the predicted slope of 0.67 from the indentation fracture mechanics model for ceramics and inorganic glasses which gives [1, 24]

$$C_0 = (\chi_r P/K_c)^{2/3} \quad (5)$$

TABLE I Comparison of the ratio of surface radial crack size ($C_0$) to plastic zone size ($r_p$) at $P = 100\,N$ for Vickers indentation of various materials

| Material | $E$(GPa) | $H$(GPa) | $C_0$($\mu$m) | $C_0/r_p$ | Ref. |
|---|---|---|---|---|---|
| Radial crack form semicircular flaw | | | | | |
| Soda–lime glass | 73 | 5.6 | 362 | 1.6 | [1] |
| $Si_3N_4$ | 300 | 18.5 | 140 | 1.0 | [1] |
| SiC | 436 | 24 | 158 | 1.3 | [1] |
| $Al_2O_3$ | 425 | 21.8 | 283 | 2.1 | [1] |
| Radial cracks form Palmqvist flaw | | | | | |
| WC–Co | 575 | 13.2 | 61 | 0.27 | [1] |
| WC–Co | 575 | 16.7 | 90 | 0.48 | [19] |
| PMMA | 3.1 | 0.21 | 770 | 0.68 | This study |

where $K_c$ is the critical stress intensity and $\chi_r$ is a constant. The smaller slope of the PMMA data indicates that for an equivalent increment of $P$, a smaller crack extension is observed in PMMA as compared to ceramics. A possible explanation for this difference in slope is that PMMA exhibits crack growth resistance behaviour in which the toughness ($K_c$) increases with increasing crack length. This crack resistance behaviour is known to exist in metals [12], alumina [25, 26], toughened ceramics [27], and polymer-filled concrete [28]. For PMMA it is generally believed that the formation of crazes in front of the crack tip plays an important role in determining the toughness. Several studies [23, 29–32] on the craze profile at crack tip in PMMA reveal that crazes form a plastic zone at the crack tip and act to arrest crack propagation. The exact mechanism by which crazing gives rise to crack resistance behaviour for indented cracks is currently being studied by the present authors.

The data in Fig. 4 can be analysed by taking toughness to be related to crack size by a simple power law relationship [12, 25]:

$$K_c = k\,C^m \quad (6)$$

where $k$ and $m$ are constants. Substituting Equation 6 into Equation 5 gives

$$C_0 = (\chi_r P/k)^{2/(2m+3)} \quad (7)$$

Based on the slope of the data in Fig. 4, $m$ is calculated to be 0.5 ($\pm$0.24). This value is higher than the value of 0.17 for aluminium alloys [12], 0.14 to 0.3 for alumina [25, 26] and 0.20 for polymer-filled concrete [28].

It should be noted that $m$ is very sensitive to the indentation load–crack size data. The uncertainty of

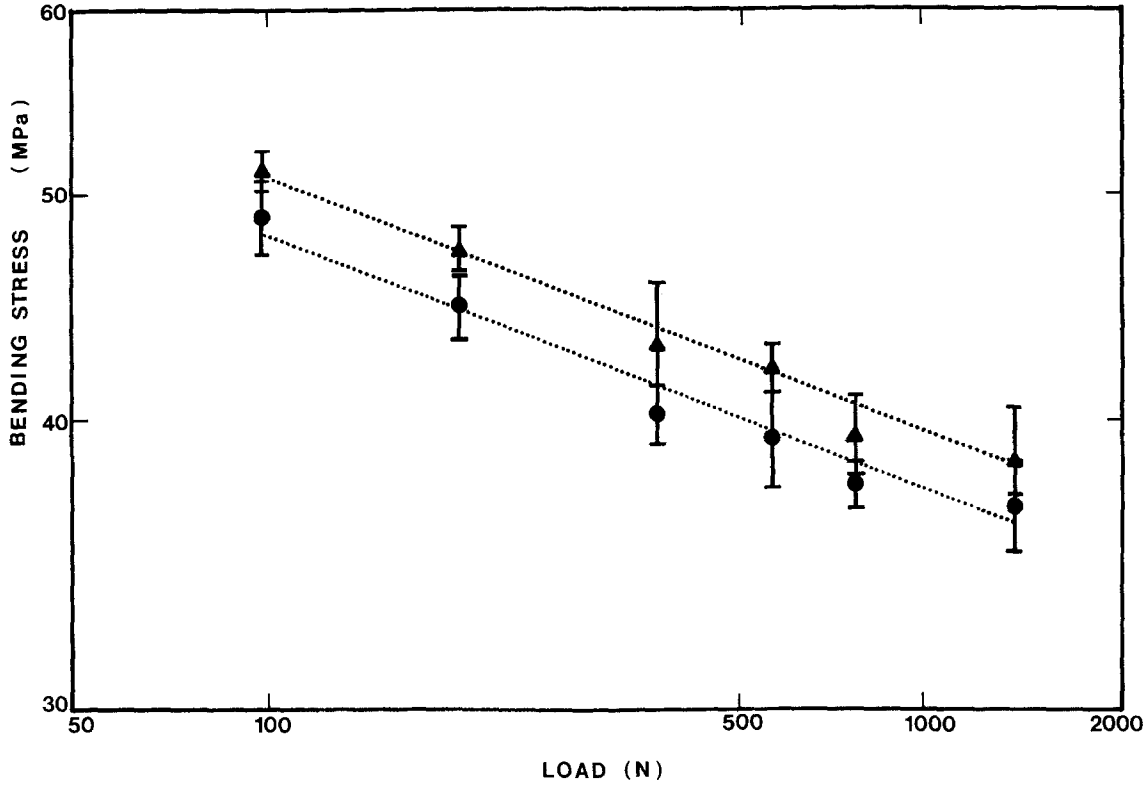


*Figure 5* Bending strength of (●) as-indented and (▲) annealed samples against indentation load.

the measured slope in Fig. 4 (0.5 ± 0.06) results in an uncertainty in $m$ from 0.26 to 0.74, which is obviously not precise enough to determine the $m$ value. The strength measurement method, as described below, is thought to be the better way to obtain the value of $m$. This is especially so when one considers the ambiguity associated with establishing exactly where the crack tip is.

### 3.3. Crack size–strength

The strength results as a function of indentation load are summarized in Fig. 5. Both the as-indented and annealed samples show a best-fit slope of $-0.113$ ($\pm 0.001$). The regression analyses give for the intercepts 1.91 ($\pm 0.004$) and 1.94 ($\pm 0.005$) for the as-indented and annealed samples, respectively. The results in Fig. 5 show that the as-indented samples are about 6% lower in strength.

The fracture surface of an as-indented sample is shown in Fig. 6. It can be seen that the plastic zone prevents the two "wings" of the Palmqvist cracks from joining up; hence, failure initiates from one individual half of the Palmqvist crack. Thus, the initial crack shape is not semicircular but is better approximated as a semi-ellipse. For all indentation loads the ratio of crack depth to radial crack size was about 0.5. Such results suggest that the Palmqvist cracks behave differently from a well-defined, semicircular flaw of similar surface trace size so far as failure is concerned. In particular, the crack depth ($d_0$) of Palmqvist cracks should be the essential flaw dimension to govern the strength of PMMA instead of the radial surface crack trace. This agrees with a previous study by Glaesemann *et al.* [33] where it was found that for indented soda–lime glass the critical crack dimension with respect to strength is the crack depth (minor axis) rather than the surface trace (major axis). Fig. 6 also shows the formation of a mirror region around the strength-

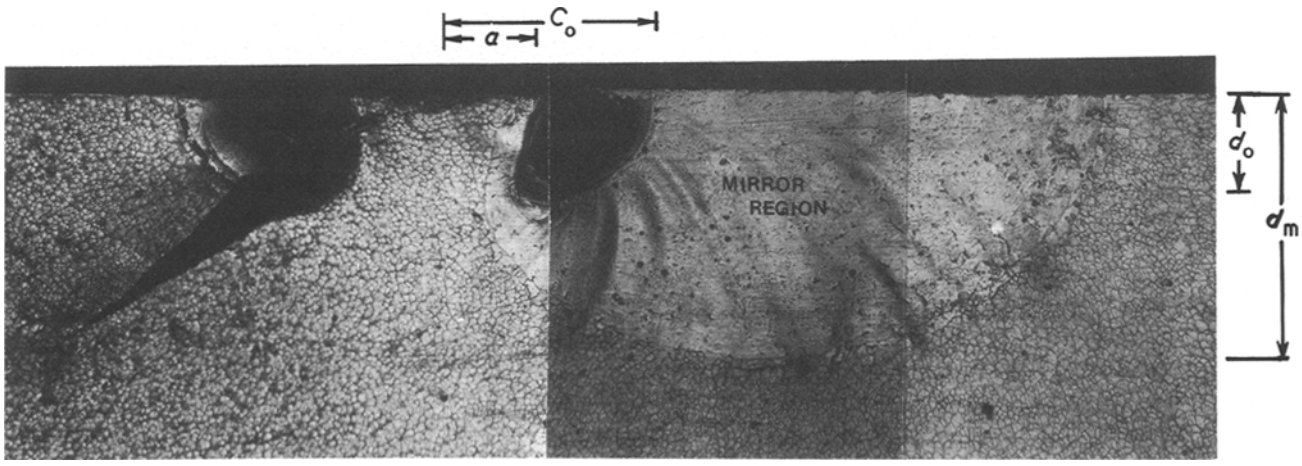


*Figure 6* Fracture surface of an as-indented sample under indentation load of 40 N and bending stress of 43.9 MPa. (27 ×).

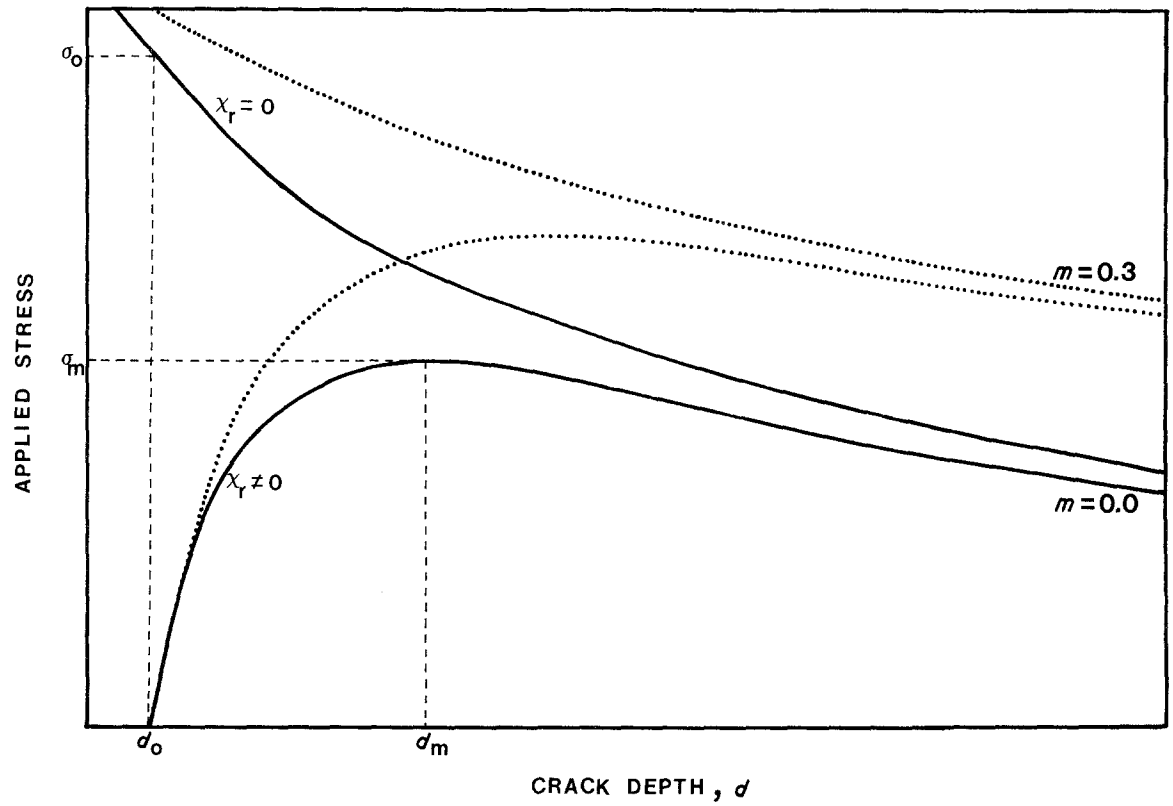


*Figure 7* Applied stress against crack depth for different $m$ (values).

controlling Palmqvist crack. This mirror fracture morphology has been seen in many glassy polymers [34, 35] and is thought to be generated from a coalescence of voids or failure of fibrils as the crack propagates through the pre-existing craze region.

During a strength test of an indented flaw, the residual force that still persists in the sample after indentation supplements the applied tension in driving the radial cracks to failure. The net stress intensity factor ($K$) is then the sum of that due to the residual force and that due to the applied stress [2, 25]:

$$K = \frac{P\chi_r}{d^{3/2}} + \Omega\sigma_a d^{1/2} \tag{8}$$

where $\sigma_a$ is the applied stress, $d$ is the Palmqvist crack depth, and $\Omega$ is a constant dependent on the geometry of the loading and flaw shape. For a semi-elliptical surface flaw ($d/C_0 = 0.5$) the maximum stress intensity is at crack depth and has an $\Omega$ value approximately equal to 1.01 [25, 36]. An applied stress–equilibrium crack size function follows from Equation 8 by putting $K = K_c$, letting from Equation 6 $K_c = kd^m$, and solving for $\sigma_a$:

$$\sigma_a = \frac{1}{\Omega d^{1/2}}\left(kd^m - \frac{\chi_r P}{d^{3/2}}\right) \tag{9}$$

A schematic plot of Equation 9 is shown in Fig. 7 for non-zero and zero $\chi_r$. For non-zero $\chi_r$ the curve exhibits a maximum at

$$d_m = \left(\frac{4\chi_r P}{k(1-2m)}\right)^{2/(2m+3)} \tag{10}$$

$$\sigma_m = \frac{k}{\Omega}\left(\frac{2m+3}{4}\right)\left(\frac{4\chi_r P}{k(1-2m)}\right)^{(2m-1)/(2m+3)} \tag{11}$$

The curves in Fig. 7 represent contrasting behaviour. For $\chi_r = 0$, failure occurs spontaneously when

$$\sigma_0 = \frac{k}{\Omega} d_0^{(2m-1)/2} = \frac{k}{\Omega}\left(\frac{\chi_r P}{k}\right)^{(2m-1)/(2m+3)} \tag{12}$$

For $\chi_r > 0$ the crack extends stably from $d_0$ to $d_m$ before failure occurs at $\sigma_m$. The relative crack extension can be obtained from a ratio of Equations 7 and 10 to be

$$\frac{d_m}{d_0} = \left(\frac{4}{1-2m}\right)^{2/(2m+3)} \tag{13}$$

The reduction in strength caused by the residual force can be calculated by taking the ratio of Equations 11 and 12:

$$\frac{\sigma_m}{\sigma_0} = \left(\frac{2m+3}{4}\right)\left(\frac{4}{1-2m}\right)^{(2m-1)/(2m+3)} \tag{14}$$

For $m = 0$, Equations 13 and 14 show that the presence of a residual force causes a relative crack extension of 2.5 and the strength decrease is 53%. For $m > 0$, the corresponding crack extension is greater but the reduction in strength is less.

Note that for $m \geqq 0.5$, there is no maximum in the applied stress–equilibrium crack length curve, Equation 9; thus, the applied stress can increase infinitely without reaching crack instability. Since this is physically impossible, $m$ must be less than 0.5. In agreement with Equations 11 and 12 the slopes ($-0.113$) of the two sets of data in Fig. 5 are equal and $m$ can be calculated to be 0.29 ($\pm 0.012$). From Equation 14 with $m = 0.29$ it follows that the strength decrease of the as-indented specimens should be 24%; however, the actual strength reduction is only about 6%. From Equation 13 with $m = 0.29$ the

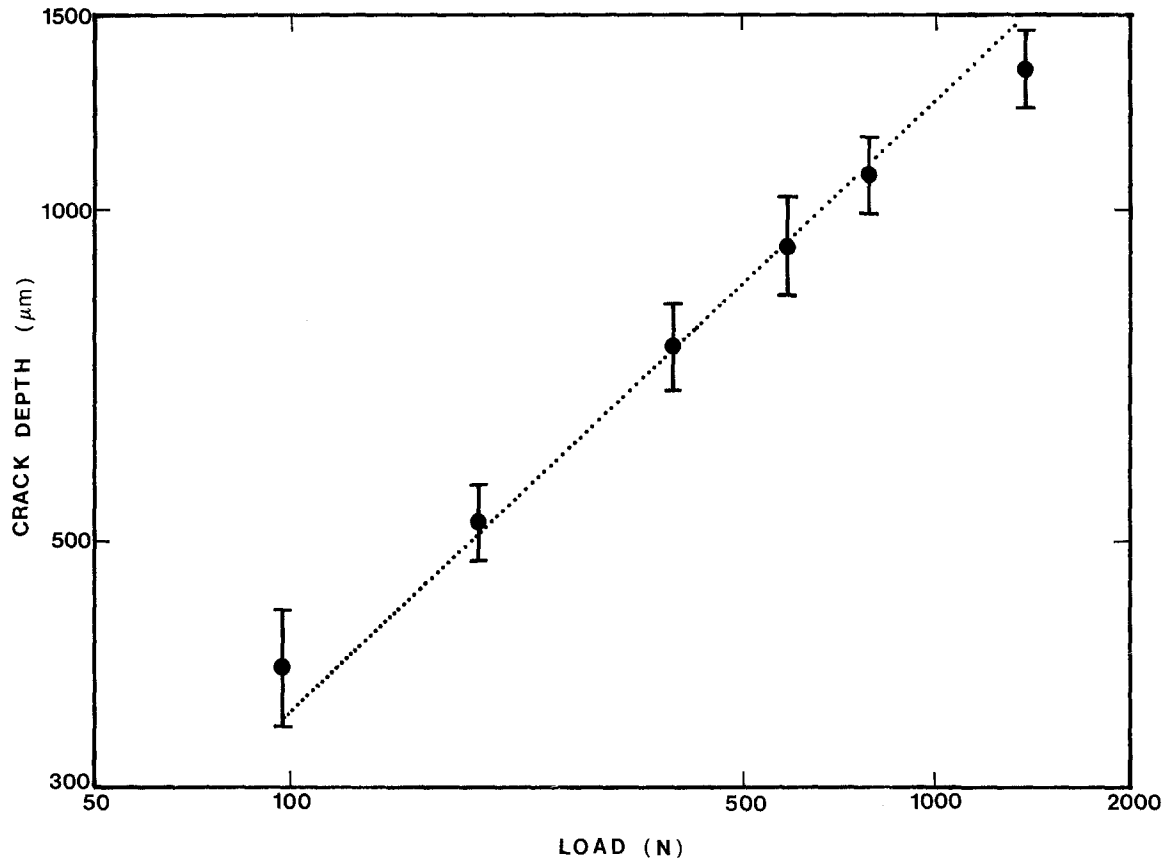


*Figure 8* Comparison of the experimental crack depth data and the prediction from strength results as a function of indentation load. (♦) Data points with standard deviation; (· · ·) predicted.

predicted crack depth at failure is 3.5 times the original crack depth. The multiple indentation–strength tests revealed that, as expected, there was no significant stable crack growth of the annealed sample prior to failure; however, for the as-indented sample, the radial crack grew to about 1.4 times the original size. These discrepancies between predicted and observed strength and extent of stable crack growth in the as-indented samples are thought to be related to such factors as stress relaxation and secondary cracking reducing the residual force field associated with the indent. Also, the power-law form for crack resistance behaviour (Equation 6) was assumed for mathematical simplicity; however, a more exact form may give better agreement.

The constants $k$ and $\chi_r$ can be determined by rewriting Equation 7 in terms of initial crack depth $d_0$:

$$d_0 = (\chi_r P/k)^{2/(2m+3)} \quad (15)$$

The initial crack depth as measured from fractography is plotted as a function of the indentation load in Fig. 8. A best-fit line with a slope of 0.56 (corresponding to $m = 0.29$) on logarithmic axes can be seen to fit the data quite well. This regressed line has an intercept of $-4.59$ ($\pm 0.03$) in SI units which from Equation 15 corresponds to $\log (k/\chi_r) = 8.21 \pm 0.06$. Substituting this $(k/\chi_r)$ ratio into Equations 12 and 13, $k$ can be calculated from the respective intercept values of the strength data in Fig. 5 taking $\Omega = 1.01$. Based on the as-indented strength, $k$ is 13.96 ($\pm 0.29$) and the associated $\chi_r$ is 0.086 ($\pm 0.002$). The annealed strength data give a $k$ of 10.32 ($\pm 0.29$) with a $\chi_r$ of 0.063 ($\pm 0.002$). The similarity in these $k$ and $\chi_r$ values gives additional support to the belief that the residual force term in Equation 8 has been properly accounted for.

From these calculated values for $k$ and $\chi_r$ the fracture resistance curve for PMMA can be calculated from Equation 6, as shown in Fig. 9. Note that crack depth was substituted for the radial crack size in Equation 6. For the range of indentation loads used in this study, the initial crack depth varied from an average of 340 to 1340 $\mu$m. Based on the as-indented data, fracture toughness over this crack size range increases from 1.42 to 2.05 MPa $m^{1/2}$, and from 1.05 to 1.51 MPa $m^{1/2}$ for the annealed data. The difference in $K_c$ values between the as-indented and annealed data is similar to that observed in soda–lime glass [37] and could be related to possible crack healing effects on annealing.

The three-point bending tests gave a $K_c$ value for this material of 1.46 ($\pm 0.11$) MPa $m^{1/2}$. There was no significant difference in the $K_c$ value, as measured on the as-notched samples compared with those that had acetone added and dried in the notch. These results indicate that the presence of acetone during indentation did not affect the subsequent strength measurement. This measured $K_c$ value from the standard fracture mechanics test falls well within the range of the $K_c$ values obtained from the indentation–strength technique and the published data (0.6 to 2.4 MPa $m^{1/2}$ in air) [23, 38]. Such a result suggests that one of the reasons for the wide range of published $K_c$ values for PMMA is the fact that PMMA exhibits crack-resistant behaviour where fracture toughness increases with crack size.

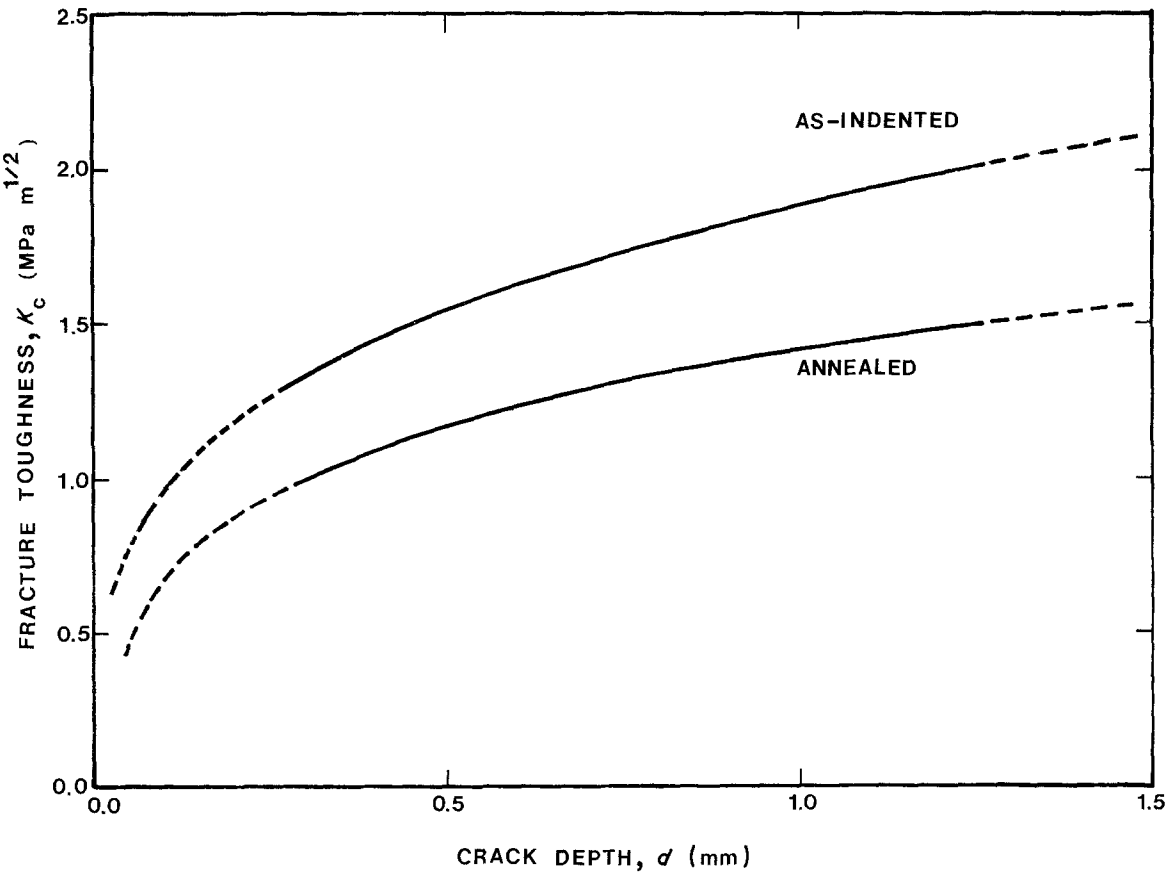


*Figure 9* Predicted fracture resistance curve for PMMA.

## 4. Conclusions

1. Crack pattern observations of Vickers indentation flaws in the PMMA/acetone system revealed that Palmqvist cracks are formed rather than semicircular median cracks. This crack geometry was found to correlate very well with the ratio of surface crack trace to indentation plastic zone size. When a material has a $C_0/r_p$ ratio greater than 1.0, a median, semicircular crack pattern is formed; while the Palmqvist crack pattern forms when the ratio is about 0.7 or less. PMMA has a ratio of 0.68.

2. Fractography of strength-tested specimens suggested that the crack depth (not the surface trace) of the Palmqvist cracks is the critical dimension that determines the strength of PMMA samples. The relationships between crack depth, indentation load, and strength were well characterized by an indentation fracture mechanics model.

3. The failure strength of both as-indented and annealed specimens showed a linear relationship with indentation load on a logarithmic plot with a slope of $-0.113$. Compared to constant fracture-toughness materials (slope $= -1/3$), this slope is about 66% less indicating that PMMA exhibits a rising fracture toughness behaviour. The range of values for the resistance curve was within the range of $K_c$ values reported in the literature.

## Acknowledgement

This research was supported by an IBM Materials and Processing Sciences grant to the Institute for Interface Science at the University of Massachusetts, Amherst.

## References

1. G. R. ANSTIS, P. CHANTIKUL, B. R. LAWN and D. B. MARSHALL, *J. Amer. Ceram. Soc.* **64** (9) (1981) 533.
2. P. CHANTIKUL, G. R. ANSTIS, B. R. LAWN and D. B. MARSHALL, *ibid.* **64** (9) (1981) 539.
3. D. B. MARSHALL, ASTM STP 844 (American Society for Testing and Materials, Philadelphia, 1984) pp. 3–21.
4. R. F. COOK and B. R. LAWN, *ibid.* pp. 22–42.
5. R. F. COOK, B. R. LAWN and G. R. ANSTIS, *J. Amer. Ceram. Soc.* **16** (10) (1981) 2846.
6. *Idem, ibid.* **14** (4) (1982) 1108.
7. B. R. LAWN, K. JAKUS and A. C. GONZALES, *ibid.* **68** (1) (1985) 25.
8. R. F. COOK, B. R. LAWN, T. P. DABBS and P. CHANTIKUL, *ibid.* **64** (9) (1981) C121.
9. J. E. RITTER, P. STRZEPA and K. JAKUS, *Phys. Chem. Glass* **25** (1986) 159.
10. D. B. MARSHALL and B. R. LAWN, ASTM STP 889 (American Society for Testing and Materials, Philadelphia, 1986) pp. 24–46.
11. K. JAKUS, J. E. RITTER Jr and C. A. LARSEN, *Polym. Eng. Sci.* **21** (1981) 854.
12. D. BROEK, "Elementary Engineering Fracture Mechanics" (Nijhoff, Netherlands, 1983) pp. 170–196.
13. B. R. LAWN, T. P. DABBS and C. J. FAIRBANKS, *J. Mater. Sci.* **18** (1983) 2785.
14. T. B. DABBS, C. J. FAIRBANKS and B. R. LAWN, ASTM STP 844 (American Society for Testing and Materials, 1984) pp. 142–153.
15. J. T. HAGAN, *J. Mater. Sci.* **14** (1979) 2975.
16. *Idem, ibid.* **15** (1980) 1417.
17. S. PALMQVIST, *Jernkontorets Ann.* **141** (1957) 300.
18. C. T. PETERS, *J. Mater. Sci.* **14** (1979) 1619.
19. D. K. SHETTY, I. G. WRIGHT, P. N. MINCER and A. H. CLAUER, *ibid.* **20** (1985) 1873.
20. R. HILL, "The Mathematical Theory of Plasticity", (Clarendon, Oxford, 1983) pp. 97–114.

21. D. M. MARSH, *Proc. R. Soc.* **A279** (1964) 420.
22. W. HIRST and M. G. J. HOUSE, *ibid.* **A311** (1969) 429.
23. S. I. ISRAEL, E. L. THOMAS and W. W. GERBERICH, *J. Mater. Sci.* **14** (1979) 2128.
24. B. R. LAWN, A. G. EVANS and D. B. MARSHALL, *J. Amer. Ceram. Soc.* **63** (1980) 574.
25. R. F. KRAUSE Jr, *ibid.* in press.
26. R. KNEHENS and R. STEINBRECH, *J. Mater. Sci. Lett.* **1** (1982) 327.
27. D. B. MARSHALL and J. E. RITTER, *Bull. Amer. Ceram. Soc.* **66** (2) (1987) 309.
28. R. F. KRAUSE Jr and E. R. FULLER Jr, in "Chevron-notched Specimens: Testing and Stress Analysis", edited by J. H. Underwood, S. W. Freiman and F. I. Baratta, (American Society for Testing and Materials, Philadelphia, 1984) pp. 309–323.
29. G. P. MORGAN and I. M. WARD, *Polymer* **18** (1977) 87.
30. H. R. BROWN and I. M. WARD, *ibid.* **14** (1973) 469.
31. W. DOLL, *Adv. Polym. Sci.* **52/53** (1983) 105.
32. W. DOLL, L. KONCZOLL and M. G. SCHINKER, *Polymer* **24** (1983) 1213.
33. G. S. GLAESEMANN, K. JAKUS and J. E. RITTER Jr, *J. Amer. Ceram. Soc.* in press.
34. H. BEVIS and D. HULL, *J. Mater. Sci.* **15** (1970) 983.
35. M. J. DOYLE, A. MARANCI, E. OROWAN and S. T. STORK, *Proc. R. Soc.* **A329**, (1972) 137.
36. J. C. NEWMAN and I. S. RAJU, *Eng. Frac. Mech.* **15** (1–2) (1981) 185.
37. J. E. RITTER Jr, F. M. MAHONEY and K. JAKUS, *Frac. Mech. Ceram.* **8** (1986) 213.
38. S. I. ISRAEL, E. L. THOMAS and W. W. GERBERICH, *J. Mater. Sci.* **15** (1980) 2389.

*Received 6 May*
*and accepted 22 July 1987*